

Research on the Vesicle–Micelle Transition by ^1H NMR Relaxation MeasurementMasumi Villeneuve,^{*,†} Rie Ootsu,[†] Mitsumasa Ishiwata,[‡] and Hiroo Nakahara[†]*Department of Chemistry, and Department of Physics, Faculty of Science, Saitama University, 255 Shimo-okubo, Sakura-ku, Saitama, 338-8570 Japan**Received: April 6, 2006; In Final Form: July 7, 2006*

We have investigated how the dynamics of surfactant molecules changes with the vesicle–micelle transition by ^1H NMR relaxation studies on the sodium decyl sulfate (SDeS)–decyltrimethylammonium bromide (DeTAB)–deuterium oxide system. The study has been planned with reference to the phase diagram of the SDeS–DeTAB–water system deduced from thermodynamic analysis of the surface tension data. The spin–lattice relaxation time (T_1) and the spin–spin relaxation time (T_2) are measured at 90 and 400 MHz at various total molalities, m , and compositions, X_2 , of the surfactants. The data were analyzed according to the “two-step” model developed by Wennerström et al. and molecular dynamics of the surfactant is discussed from the viewpoint of correlation time τ_f associated with the local fast motion of the surfactant molecule, correlation time τ_s associated with the slow overall motions of the aggregate and surfactant molecules within it, and local order parameter S . We find τ_s of vesicles is an order of magnitude larger than that of micelles signifying that the tumbling of vesicle particles and surfactant diffusion over the vesicle are much slower than those for micelle. τ_f and S for vesicles are also larger than those for micelles. Molecular environments of the surfactant are also discussed from the dependence of the chemical shifts on m at constant X_2 or from that on X_2 at constant m . When the chemical shifts in vesicle and micelle are compared at constant m , the chemical shifts in vesicle are displaced to a lower magnetic field than those in micelle, which implies that the surfactant molecules are arranged more closely to each other in the vesicle than in the micelle.

1. Introduction

Surfactant molecules associate into a variety of structures in aqueous solutions which can transform from one to another when the solution conditions are altered, e.g., surfactant concentration, mixing ratio of binary surfactants, electrolyte concentration, pH, temperature, or pressure. These aggregate structures are utilized in different technologies. It is nearly 20 years since vesicle was clarified to be one of the spontaneously formed equilibrium structures by the pioneering work of Kaler et al.¹ Since then the spontaneous vesicle has become one of the most popular topics in the field of colloid and interface science. Among such spontaneous vesicle systems, especially binary anionic–cationic surfactant systems have attracted much attention because they exhibit a wide variety of structures in addition to the vesicles depending on the total concentration and the mixing ratio of the surfactants. Among the extensive studies on phase behavior of the binary anionic–cationic surfactant mixture, we have clarified the detailed phase diagram in the vicinity of the water corner of the Gibbs triangle and shown that vesicle coexists with micelle in a certain condition for the first time by careful measurement of the surface tension and thermodynamic analysis of the data.² However, only a few investigations have ever been carried out about the dynamics of surfactant molecules in vesicle and micelle of such systems.³ Molecular motion is related to the character of aggregates and hence it is important to understand the self-assembly from the viewpoints of dynamics as well as thermodynamics.

It is well-known that the nuclear magnetic resonance (NMR) is a powerful tool to explore microscopic behavior and dynamics of molecules constituting the aggregate.^{3,4,6–12} The self-diffusion coefficient D measured by the pulse gradient NMR gives an effective radius of the molecular assembly. The spin–lattice relaxation time T_1 and the spin–spin relaxation time T_2 provide information on the molecular motion quantified in terms of the correlation time τ . Furthermore, T_2 and the chemical shift give a time scale of the exchange of a surfactant molecule between different environments. Since molecular motions of the aggregate and the entire surfactant molecule within it are fairly slow, relaxation data of the aggregates depend on the Larmor frequency. To analyze such data, several models have been proposed, for example, by Wennerström et al.^{4,5} and by Lipari and Szabo.¹³ Their approaches have been adopted in numerous studies concerning micelle. These models divide the thermal motion into contributions from fast and slow modes. In this study, we use the “two-step” model developed by Wennerström et al.

The purpose of this study is, first, to investigate how the molecular dynamics changes with the vesicle–micelle transition, and second, to understand the effect of solution environment on the dynamics. In this study, we focus on the sodium decyl sulfate (SDeS)–decyltrimethylammonium bromide (DeTAB)–deuterium oxide (D_2O) system, making reference to the phase diagram previously obtained for the SDeS–DeTAB–water (H_2O) system² reproduced in Figure 1 with the total molality m and the composition X_2 defined below by eqs 1 and 2, respectively, differently from the previous work (note that in the literature, the total molality \hat{m} and the composition \hat{X}_2 are defined so as to take into consideration dissociation of the electrolytes). The hatched area in Figure 1 shows the region

* Address correspondence to this author. E-mail: villeneuve@chem.saitama-u.ac.jp.

[†] Department of Chemistry.

[‡] Department of Physics.

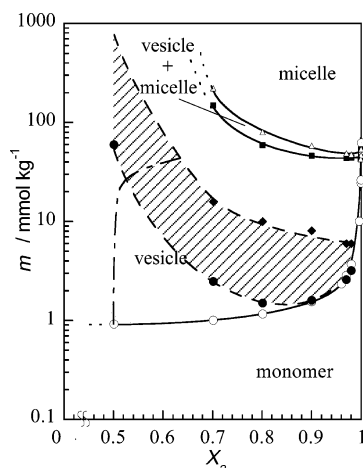


Figure 1. Phase diagram of aggregate formation at 298.15 K: (○) CVC vs X_2 curve; (—•—) CVC vs X_2^V curve; (■) concentration where micelles appear in the vesicle solution vs X_2 curve; (Δ) concentration where vesicles disappear from the vesicle–micelle coexisting solution vs X_2 curve; the hatched area indicates the region where vesicles flocculate to give powdery suspension.

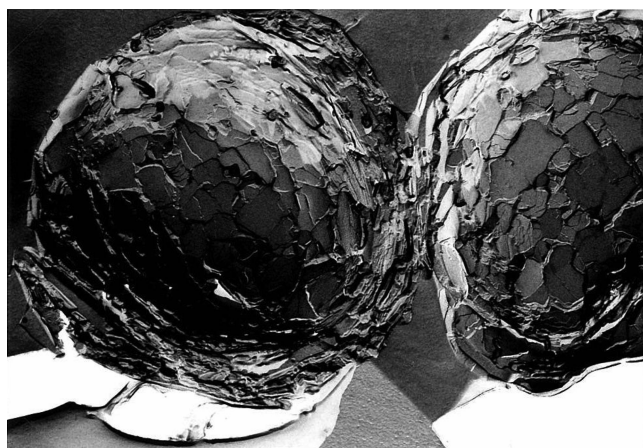


Figure 2. A FF-TEM image taken in the SDeS–DeTAB–H₂O system at $X_2 = 0.70$ and $m = 14 \text{ mmol kg}^{-1}$. Scale bar = $1 \mu\text{m}$. The micrograph suggests that the powdery suspension is flocculated vesicles.

where powdery suspension is formed, which tends to gather on top of the solution. The powder consists of densely packed vesicle particles as shown by the FF-TEM micrograph in Figure 2, taken at $X_2 = 0.70$ and $m = 14 \text{ mmol kg}^{-1}$.

Here let us briefly explain Figure 1. In the SDeS–DeTAB–H₂O system, when m is increased along $X_2 = 0.78$, the surfactants transform from monomers to vesicles of initial composition of $X_2^V = 0.5$ at $m = 1.15 \text{ mmol kg}^{-1}$, which is the critical vesicle concentration (CVC) at $X_2 = 0.78$, and then the vesicles flocculate to form powdery suspension at $m = 1.59 \text{ mmol kg}^{-1}$. Further increment of m disperses the vesicles again at $m = 9.84 \text{ mmol kg}^{-1}$. At $m = 64.97 \text{ mmol kg}^{-1}$, micelles appear in the vesicle solution and up until $m = 92.94 \text{ mmol kg}^{-1}$ vesicles and micelles coexist in the solution. At $m = 92.94 \text{ mmol kg}^{-1}$, vesicles completely disappear from the solution and above this concentration almost all surfactants exist as micelles. Along $X_2 = 0.95$, CVC is $m = 2.06 \text{ mmol kg}^{-1}$ and vesicles flocculate at around $m = 2.20 \text{ mmol kg}^{-1}$, they redisperse at $m = 6.44 \text{ mmol kg}^{-1}$, then micelles start to form at $m = 43.97 \text{ mmol kg}^{-1}$ and vesicles disappear at $m = 50.08 \text{ mmol kg}^{-1}$. On the other hand, as m is increased along $X_2 = 1$, surfactants

only transform from monomers to micelles at the critical micelle concentration (CMC) of $m = 62.80 \text{ mmol kg}^{-1}$. When X_2 is decreased from 1 to 0.5, for example, along $m = 100.00 \text{ mmol kg}^{-1}$, vesicles start to form in the micellar solution at $X_2 = 0.78$ and micelles coexist with vesicles down until $X_2 = 0.74$ where the surfactants completely transform to vesicles. As X_2 is further decreased, the vesicles flocculate at around $X_2 = 0.59$. Whereas when X_2 is decreased from 1 along $m = 30.00 \text{ mmol kg}^{-1}$, surfactants transform from monomers to vesicles between $X_2 = 1$ and 0.9999, then down at $X_2 = 0.66$ they start to flocculate.

2. Experimental Section

2.1. Material. SDeS was synthesized according to the literature¹⁴ and recrystallized first from a mixture of ethanol and butanol (w/w 3:1) three times and subsequently from ethanol. DeTAB (99.0%) was purchased from Tokyo Kasei Kogyo Co., Ltd. (Japan), and purified by recrystallization from a mixture of acetone and ethanol (w/w 4:1) four times. Deuterium oxide (99.9% ²H) was purchased from either Sigma-Aldrich Co. (USA) or Wako Pure Chemical Industries Ltd. (Japan). The purity of the surfactants was confirmed by ¹H NMR spectra and by surface tension measurement of their aqueous solutions. The critical micelle concentrations (CMC) of the purified surfactants coincided with the literature and there were no minima on the surface tension vs concentration curves in the vicinity of CMC. At the beginning of the study, some experiments were done with sodium 3-(trimethylsilyl)-1-propane sulfonate (TSPSA) as an external reference for the chemical shifts. TSPSA was purchased from Aldrich Chem. Co. (USA). Later, we utilized the signal of HDO as an internal reference of the chemical shifts.

2.2. Sample Preparation. All sample solutions were prepared by dispersing a mixture of dry surfactants into D₂O, and they were never sonicated.

Total molality m and composition X_2 of the mixed surfactant solution are defined by the following equations

$$m = m_1 + m_2 \quad (1)$$

and

$$X_2 = m_2/m \quad (2)$$

where m_1 and m_2 are molalities of SDeS and DeTAB, respectively.

2.3. Measurement. **2.3.1. NMR.** All the measurement was carried out at $298.2 \pm 0.5 \text{ K}$. NMR measurement was performed by a Bruker DRX400 with a 9.40 T superconducting electromagnet, and a JEOL FX90Q with a 2.11 T electromagnet, both of which are Fourier transform spectrometers. Their resonance frequencies $\omega/(2\pi)$ of ¹H are 89.5 and 400.13 MHz for FX90Q and DRX400, respectively. To keep a homogeneity of the static magnetic field for a long time, internal lock of D₂O was used in both spectrometers. The chemical shifts of all ¹H NMR spectra are reported in ppm as δ relative to TSPSA. T_1 was measured by the inversion–recovery pulse sequence (pulse delay (PD)–180°_x– τ –90°_x–acquisition (AC)). T_2 was measured by the Carr–Purcell–Meiboom–Gill (CPMG) sequence (PD–90°_x–[τ –180°_y– τ]_{2n}–AC).

However, for the vesicle solution, T_2 is too short to be determined experimentally, therefore, T_2 values of vesicle solutions were estimated from the line widths at half-height, $\Delta\nu_{1/2}$, of the resonance signals. Because the experimental half-height width comprises the contribution of inhomogeneity of the magnetic field as well as that of true transverse relaxation,

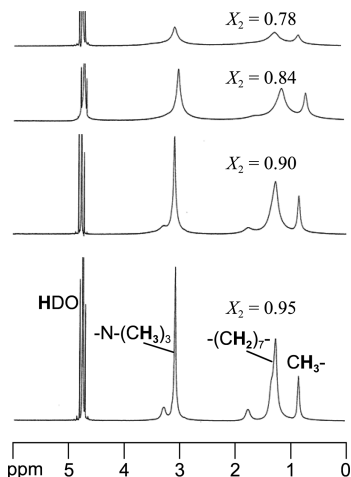


Figure 3. Proton NMR spectra of vesicle solutions of $m = 30 \text{ mmol kg}^{-1}$ measured at 400 MHz and 298.2 K. The chemical shifts are expressed with respect to TSPSA. The presence of vesicle in the solution broadens the spectral lines. The line widths enlarge as X_2 approaches 0.5.

the inhomogeneous line width was estimated for each spectrometer by comparing T_2 of a micellar solution measured by the CPMG method and that calculated from the observed line width. Furthermore, since the line widths of ^1H NMR spectra for vesicular solutions are fairly broad as shown in Figure 3, it is difficult to directly evaluate the line width at half-height. Hence, we decomposed the partially overlapped ^1H spectra by computer with the aid of NMR Utility Transform Software (NUTS) for Windows 95/NT released by Acorn NMR Co. (USA).

T_1 and T_2 measurement was performed at various points along the lines of constant composition at $X_2 = 0.78, 0.95$, and 1 and along the lines of constant total molality at $m = 30, 100, 152$, and 265 mmol kg^{-1} in both of the magnetic fields.

It is well-known that dissolved oxygen can shorten the relaxation times. This paramagnetic effect is known to be greater as the relaxation time of the nucleus is longer. We measured both degassed and undegassed samples of the longest T_1 and T_2 . No differences were observed with and without degassing therefore the measurement was carried out without it.

To evaluate hydrodynamic radii of micelles, the self-diffusion coefficients were measured on DRX400 by the pulsed gradient field spin-echo (PGSE) technique with a single gradient (Z). The gradient strength was calibrated by using a $\text{H}_2\text{O}/\text{D}_2\text{O}$ mixture in which a Teflon block with two holes separated vertically by 10 mm was inserted. Diffusion coefficients were measured by increasing the amplitude of the field gradient pulses in 32 steps ($0.67\sim 32.03 \text{ G cm}^{-1}$). The duration of gradient pulse and the diffusion time were 3 ms and 100 ms, respectively. The delay time between scans was 15 s. No restricted diffusion was observed for all the samples. Since CVC of the mixed solution is extremely low, the monomer contribution is negligible.

2.3.2. Freeze-Fracture Transmission Electron Microscopy (FF-TEM). Aqueous mixtures of SDeS and DeTAB at $X_2 = 0.70$, $m = 14 \text{ mmol kg}^{-1}$ and $X_2 = 0.70$, $m = 139 \text{ mmol kg}^{-1}$ were observed by FF-TEM to characterize the bilayer-based structures. Freeze-fracture replicas of the samples were observed with a CEM 902 electron microscope (Zeiss, Oberkochen, Germany). For the preparation of the replica, a small amount of sample was placed on a 0.1 mm thick copper disk covered by another copper disk. It was plunged into liquid propane that was precooled by liquid nitrogen. The frozen sample was

fractured and replicated in a BAF 400 (Bal-Tec, Balzer, Liechtenstein) at -140°C . The Pt/C layer was deposited at an angle of 45° .

2.3.3. Dynamic Light Scattering (DLS). DLS of the vesicle solution of the SDeS–DeTAB– H_2O system at $X_2 = 0.50$ and $m = 2.0 \text{ mmol kg}^{-1}$ was measured by an ALV/DLS/SLS-5000 Compact Goniometer System (ALV-GmbH, Germany). The light source was an LD exciting Nd:YAG Laser (532 nm, 100 mW) (Coherent Co., USA) at 298.2 K. Measurement was performed at every 5° from 50° to 150° of the scattering angle. The time correlation function of scattering intensity was expanded by the cumulant series.

2.4. Analysis of NMR Data. **2.4.1. ^1H Spin–Lattice Relaxation Time and Spin–Spin Relaxation Time.** In the case of proton NMR for the surfactant molecule, a dominant mechanism of relaxation is the intramolecular magnetic dipole–dipole interaction between geminal protons. The spin–lattice relaxation and the spin–spin relaxation time of ^1H are given in the form of

$$T_1^{-1} = A[J(\omega) + 4J(2\omega)] \quad (3)$$

and

$$T_2^{-1} = \frac{1}{2} A[3J(0) + 5J(\omega) + 2J(2\omega)] \quad (4)$$

respectively.¹⁵ Here, A is given by

$$A = \left[\frac{3(N-1)}{20} \right] \left[\frac{\mu_0 \gamma_{\text{H}}^2 \hbar}{4\pi r_{\text{H-H}}^3} \right]^2 \quad (5)$$

and ω is the Larmor frequency of the equivalent geminal protons, $J(\omega)$ is the reduced spectral density evaluated at ω for molecular motions of the internuclear vector $\vec{r}_{\text{H-H}}$ connecting a pair of interacting protons, N is the number of geminal protons, μ_0 is the magnetic permeability of vacuum, γ_{H} is the gyromagnetic ratio of proton, and $r_{\text{H-H}}$ is the distance between geminal protons.

2.4.2. The Two-Step Model. For large molecules or surfactant aggregates, NMR relaxation times are in general dependent on ω . The relaxation times are determined by the thermal motion of $\vec{r}_{\text{H-H}}$ in surfactant molecules comprising the aggregate. This thermal motion consists of various molecular motions with different characteristic time scales. In the assemble of surfactant molecules, they are classified into two types. One is slow motion with a correlation time on the order of nanoseconds, which is due to tumbling of aggregates and lateral diffusion of surfactant molecules within the aggregate, and the other is fast local motion, having a correlation time in the picosecond range, due to bond rotation, torsion, and libration, in which the surfactant molecule cannot rotate freely because of the anchoring of the headgroup at the surface of the aggregate. Therefore, it is reasonable to assume that the relaxation takes place in two steps. Assuming that (1) the two modes of motion are mutually independent, (2) the fast motion is in the extreme narrowing limit, and (3) the slow motion is isotropic, T_1 and T_2 are given by^{4,5,18}

$$T_1^{-1} = 10A\tau_f(1 - S^2) + 2AS^2 \left[\frac{\tau_s}{1 + (\omega\tau_s)^2} + \frac{4\tau_s}{1 + (2\omega\tau_s)^2} \right] \quad (6)$$

and

$$T_2^{-1} = 10A\tau_f(1 - S^2) + AS^2 \left[3\tau_s + \frac{5\tau_s}{1 + (\omega\tau_s)^2} + \frac{2\tau_s}{1 + (2\omega\tau_s)^2} \right] \quad (7)$$

Here, τ_s is the correlation time for the slow motion and τ_f is the correlation time for the fast motion of \vec{r}_{H-H} .^{8,10,18} The fast motion is complex and is not completely isotropic, and therefore not rigorously characterized by a single correlation time. However, the motion is not highly anisotropic and previous works of Söderman et al. have shown that the use of a single correlation time is appropriate.^{7,19} Although thermal motion of the aggregate itself is random in the isotropic solution, each of the aggregates has a definite form as an assembly of the surfactant molecules. Thus, an array of surfactant molecules has order in the aggregate. The parameter S expresses the degree of the order for the internuclear vector \vec{r}_{H-H} , which originates in reorientation of the surfactant molecules in the aggregate.

In this work, S , τ_f , and τ_s of protons in the surfactant molecule are evaluated by use of relaxation times T_1 and T_2 measured in the two static magnetic fields. The solution for each proton is obtained by searching the value that makes the error sum between the experimental relaxation time and the calculated one minimum in the least-squares sense. Although the correlation time τ_s is in principle independent of a segmental position observed, the τ_s value that gives the minimum error sum is slightly different from one proton to another. Therefore, the minimum and the maximum of each τ_s shown by the error bars in Figures 5, 7, 12, and 14 correspond to the error range of the τ_s .

3. Results and Discussions

Changing the solvent from H₂O to D₂O does not alter the phase diagram greatly except that CMC of pure DeTAB is lower and the coexisting region of vesicle and micelle is extended slightly in the D₂O system. The appearances of the vesicle solutions in the SDeS–DeTAB–D₂O system are very much similar to those in the SDeS–DeTAB–H₂O system studied previously.

Typical ¹H spectra of the SDeS–DeTAB–D₂O system obtained at 400 MHz for the vesicle solutions at $m = 30$ mmol kg^{−1} are shown in Figure 3. The existence of vesicle in the solution broadens the lines of all the spectra. This fact is probably due to three factors, i.e., various curvatures of the multiply bilayered vesicles, the liquid-crystal-like nature in the vesicle interior, and polydisperse distribution of the vesicular size. The first two are clearly indicated by the polarizing micrographs.¹⁶ Furthermore, the polydispersity index, defined by the quotient of the second cumulant divided by the first cumulant of the dynamic light scattering data, of the SDeS–DeTAB–H₂O system is ca. 1, which implies considerable polydispersity compared with the cetyltrimethylammonium bromide–sodium dodecylbenzenesulfonate system (ca. 0.2) studied by Kaler et al.¹⁷ Additionally, we notice that the spectrum becomes broader as X_2 approaches 0.5, which implies an increase in the number of bilayers comprising vesicle and in the vesicular size with increase of the SDeS ratio. In this study, we focus analysis of the NMR data on protons in two kinds of methyl groups, i.e., one at the end of the alkyl chain (CH₃–) and the other in the hydrophilic group (–N–(CH₃)₃), and on protons in methylenes (–(CH₂)₇–) as assigned in Figure 3.

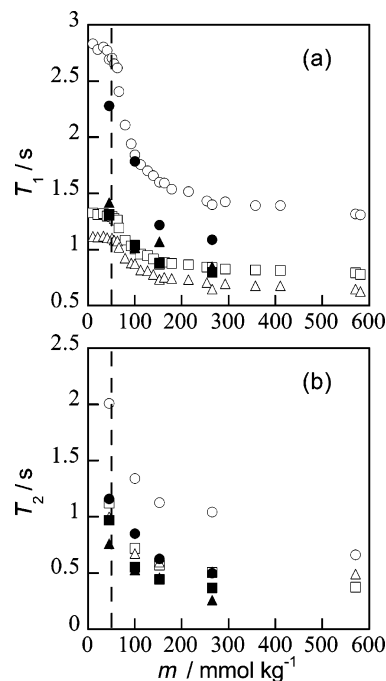


Figure 4. Relaxation times vs molality plots measured at 400 MHz for the pure DeTAB deuterium oxide solution: (a) spin–lattice relaxation time vs m ; (b) spin–spin relaxation time vs m ; (○) CH₃–; (□) –(CH₂)₇–; (△) –N(CH₃)₃; open symbols represent experimental values and filled symbols represent recalculated values from S , τ_f , and τ_s shown in Figure 4; the dashed vertical line indicates CMC.

3.1. Dynamics of the Pure DeTAB Deuterium Oxide Solution. For the pure DeTAB solution, the relaxation times T_1 and T_2 measured at 400 MHz are plotted against m in Figure 4, panels a and b, respectively. The broken line is drawn at CMC in each figure. In the D₂O solution, CMC of DeTAB is reduced to 50 mmol kg^{−1} from 63 mmol kg^{−1} in the aqueous solution. T_1 values are found to be almost independent of m up until CMC. When m reaches CMC, T_1 values of protons on all the segments decrease steeply with increasing m and become nearly constant in the high concentration range above 250 mmol kg^{−1}. Similar behavior is also seen for T_1 values measured at 90 MHz and T_2 values measured at both 90 and 400 MHz. The relaxation times of aggregate solutions are longer as ω is higher.

Additionally, the relaxation times of monomer solutions show small but definite dependence on ω . This fact suggests that monomer surfactants form a relatively large structure with D₂O most probably due to hydration. Therefore, the two-step model was applied also to analysis of the monomer data. Since CMC of DeTAB is relatively high, the monomer contribution to the observed relaxation times is substantial. In evaluating S , τ_f , and τ_s in the micellar region, the monomer contribution was subtracted by use of the following equation assuming the pseudophase separation model to obtain intrinsic relaxation times of the micelle

$$\frac{1}{T_{j,m}} = \left[\frac{1}{T_j} - \frac{m_{\text{CMC}}}{m} \left(\frac{1}{T_{j,l}} \right) \right] / \left(\frac{m - m_{\text{CMC}}}{m} \right) \quad (8)$$

where $j = 1$ or 2 , T_j values are observed relaxation times, and $T_{j,m}$ and $T_{j,l}$ are micellar and monomer relaxation times, respectively.

Numerical values of S , τ_f , and τ_s obtained from the two-step model for spherical micelles are plotted in Figure 5, panels a, b, and c, respectively. The broken lines show CMC. It is clearly seen that S and τ_f increase greatly with micelle formation. On

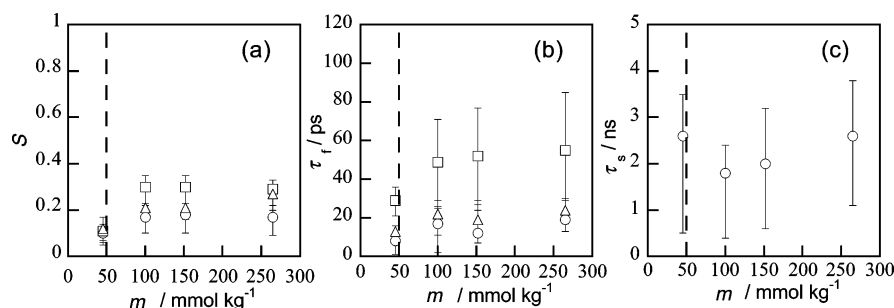


Figure 5. (a) Order parameter S vs m plots of the pure DeTAB deuterium oxide solution; (b) fast correlation time τ_f vs m ; (○) CH_3- ; (□) $-(\text{CH}_2)_7-$; (△) $-\text{N}(\text{CH}_3)_3$; (c) slow correlation time τ_s vs m ; the dashed vertical line indicates CMC.

the other hand, τ_s is almost constant at all m . Therefore, it is concluded that surfactant molecules are orderly arrayed in micelle and the fast local motion of a surfactant molecule is slower in micelle than in the monomer solution, whereas the slow overall motions of a micelle particle and a free hydrated monomer in the solution are in nearly the same extent of rate. As is shown by the quantitative analysis of the relaxation data, the reduction of T_1 and T_2 in micelle is explained by increase in the intramolecular magnetic dipole–dipole interaction due to slowing down of fast local motion of the segments accompanying growth of the local order in the process of micelle formation. The growth of the local order promotes the relaxation rate due to the slow collective motion of the whole aggregated particle such as micelle. Since the local motion of the CH_3- segment is the fastest between the segments in the monomer region, the reduction of its T_1 and T_2 values with the micelle formation is prominent as compared to that of the other segments. It is considered that CH_3- segments are highly crowded and near each other in micelle because they are in the center of the micelle.

Furthermore, Figure 4 shows relaxation times recalculated by eqs 6 and 7 from S , τ_f , and τ_s values in Figure 5. Although discrepancies, especially in the CH_3- segment, are seen between the experimental and calculated relaxation times, S , τ_f , and τ_s values well reproduce the dependence of the experimental relaxation times on m . Therefore, we confirm that the analysis by means of the two-step model is successful. The difference between the values obtained by experiment and calculation is due to the numerical errors of S , τ_f , and τ_s .

3.2. Dynamics of Mixed Vesicle and Mixed Micelle. 3.2.1.

Dependence of Molecular Mobility on m at Constant X_2 . Relaxation data of T_1 and T_2 measured at 400 MHz are plotted against m at $X_2 = 0.78$ in Figure 6, panels a and b, respectively. The broken lines are to show the phase boundaries in each figure. In the mixed surfactant solution, vesicle formation occurs at a very low concentration, micelle forms in the vesicle solution at around $m = 70 \text{ mmol kg}^{-1}$, and then vesicles completely disappear from the solution at around $m = 100 \text{ mmol kg}^{-1}$. As clearly seen in the T_1 vs m plot, T_1 values of micelles and vesicles are considerably shorter than those of monomers ($m \lesssim 1 \text{ mmol kg}^{-1}$). From the detailed analysis as shown in Figure 7, this result comes from slowing down in the slow motion of the aggregates and the surfactants therein. Since the slow motion appears with aggregation of surfactant molecule, efficiency of relaxation rises with the extent of aggregation.

In the vesicular region ($m = 1\text{--}70 \text{ mmol kg}^{-1}$), T_1 values of all the segments have similar values and are independent of m , while T_2 value are much shorter than T_1 values, which corresponds to the broad line widths shown in Figure 3. The total molality $m = 100 \text{ mmol kg}^{-1}$ is the border between the vesicle–micelle coexisting region and the micellar one. In the

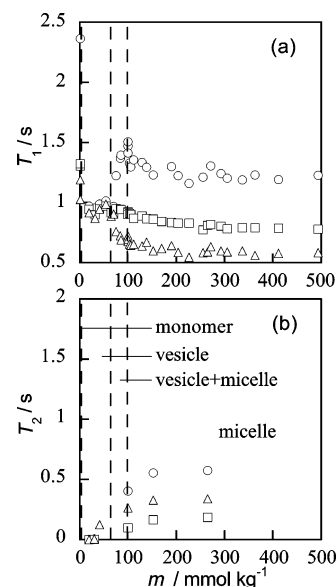


Figure 6. Relaxation times vs total molality plots of the SDeS–DeTAB– D_2O system at surfactant composition of $X_2 = 0.78$ measured at 400 MHz: (a) spin–lattice relaxation time vs m ; (b) spin–spin relaxation time vs m ; (○) CH_3- ; (□) $-(\text{CH}_2)_7-$; (△) $-\text{N}(\text{CH}_3)_3$; the dashed vertical lines indicate the phase boundaries.

vesicle–micelle coexisting region, T_1 of CH_3- becomes longer gradually with increasing m , and attains the maximum of 1.5 s at the border, and then it falls down to 1.3 s at the entrance of the micellar region. On the other hand, T_1 values of $-(\text{CH}_2)_7-$ and $-\text{N}(\text{CH}_3)_3$ segments become a little shorter with increasing m in the coexisting region. This complex behavior of T_1 for the segments in this coexisting region may reflect changes in their respective local motions with changing m in the intermediate and locally disordered phases. In the micellar region ($m > 100 \text{ mmol kg}^{-1}$), T_1 values of all the segments decrease slowly with increasing m and they reach respective constant values at $m > 200 \text{ mmol kg}^{-1}$.

On the other hand, T_2 of every segment becomes monotonically longer on the phase transition from vesicle to micelle by way of the coexisting region. Since the vesicular T_2 is very short, this increase in T_2 corresponds to the disappearance of vesicles and the growth of micelle population. The large difference between T_1 and T_2 values especially in the vesicular region results from the difference of the relaxation pathways in the two processes. Only the T_2 process involves the spectral density of $J(0)$ at $\omega = 0$, which corresponds to the distribution of the static component of the local dipolar field parallel to the static magnetic field H_0 due to the companion in the geminal protons. The large contribution of $J(0)$ to T_2 is related to the three factors mentioned for Figure 3 in connection with the broad line width in the vesicular region, namely, (1) various curvatures of the

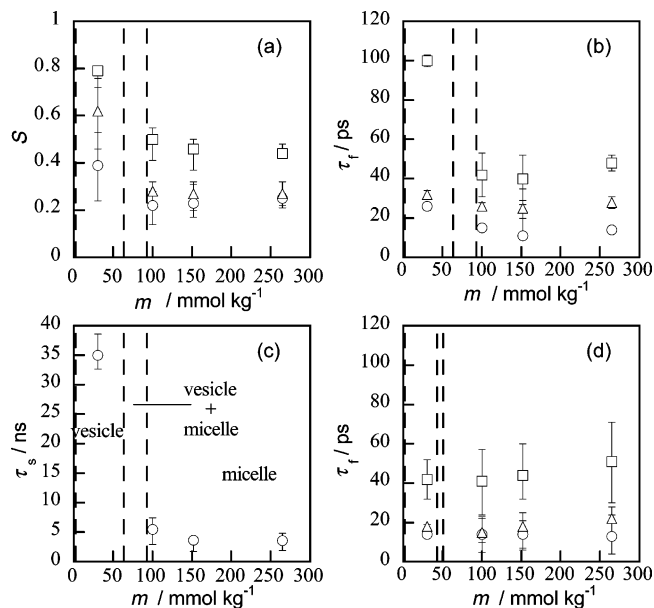


Figure 7. (a) Order parameter vs m plots of the SDeS–DeTAB–D₂O system at $X_2 = 0.78$; (b) fast correlation time vs m ; (○) CH₃–; (□) –(CH₂)₇–; (Δ) –N(CH₃)₃; (c) slow correlation time vs m ; (d) fast correlation time vs m at $X_2 = 0.95$; the dashed vertical lines indicate the phase boundaries.

multiply bilayered vesicles, (2) the liquid-crystal-like nature in the vesicle interior, and (3) polydisperse distribution of the vesicular size. In the present case, we obtain $T_2^{-1} \approx (3/2)AJ(0) = 3AS^2\tau_s$ with the calculated values of S , τ_f , and τ_s from eq 7. As shown in Figure 7, the large vesicle particle has a long slow correlation time $\tau_s = 35$ ns, which is an order of magnitude larger than those for the micelle and the monomer. This long correlation time together with the large S value in the vesicle region make T_2 considerably shorter than T_1 . The constant values of T_1 and T_2 in the high total molality range suggest that the micellar composition and the aggregate number are unchanged despite an increase of the total molality.

Although not shown in the figures, similar trends are observed for T_1 and T_2 vs m at the alternative composition of $X_2 = 0.95$.

Let us now look at the dependence of the three parameters on m in detail. In Figure 7, panels a, b, and c, S , τ_f , and τ_s vs m at $X_2 = 0.78$ plots are shown, respectively. The low total molality region is the vesicle solution. Values of S and τ_s in the vesicle region are much larger than those in the micelle region. Therefore, the slow motion, i.e., tumbling of vesicle particles and surfactant diffusion inside the vesicle, is slower compared to that of micelle irrespective of the total molality and the fraction of contribution of the slow motion is larger in the former than in the latter.

Additionally, τ_f vs m at $X_2 = 0.95$ is plotted in Figure 7d. As shown by the broken lines in the figures, the vesicle–micelle coexisting region is narrower at $X_2 = 0.95$ than at $X_2 = 0.78$. In Figure 7d, the τ_f value of the fast motion for each segment in the vesicle at $X_2 = 0.95$ takes the same value as those in the micellar region, and thus local motions such as libration, torsion, and bond rotation of the surfactant molecules in vesicle are similar to those in the micelles. However, as seen in Figure 7b, at $X_2 = 0.78$ τ_f of –(CH₂)₇– is distinctly longer for vesicle than for micelle and in addition, τ_f values of the segments at both ends of the surfactant (CH₃– and –N(CH₃)₃) are also prolonged a little. A plausible explanation is that the multilamellar vesicle formed at $X_2 = 0.78$ consists of more layers and its interior is more similar to smectic liquid crystal than the vesicle formed at $X_2 = 0.95$.

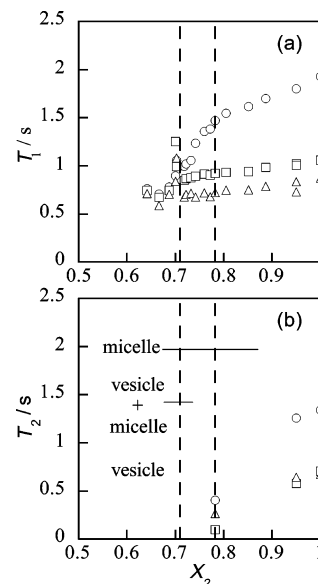


Figure 8. Relaxation times vs surfactant composition plots of the SDeS–DeTAB–D₂O system at $m = 100$ mmol kg^{−1} measured at 400 MHz: (a) spin–lattice relaxation time vs X_2 ; (b) spin–spin relaxation time vs X_2 ; (○) CH₃–; (□) –(CH₂)₇–; (Δ) –N(CH₃)₃; the dashed vertical lines indicate the phase boundaries.

3.2.2. Dependence of Molecular Mobility on X_2 at Constant m . Now, let us discuss the dependence of T_1 and T_2 on X_2 at a constant total molality to investigate the effect of structural change of the aggregate at a nearly constant ionic strength on the relaxation processes. T_1 and T_2 values of the three segments are plotted against X_2 at $m = 100$ mmol kg^{−1} in Figure 8, panels a and b, respectively. There appear clearly two bends on the T_1 vs X_2 plot of the CH₃– segment at $X_2 = 0.71$ and 0.78 , which is considered to correspond respectively to the beginning and the end of the vesicle–micelle coexisting region in the SDeS–DeTAB–H₂O system is determined to be $X_2 = 0.74–0.78$ as shown in Figure 1, in the SDeS–DeTAB–D₂O system, such a coexisting region is found to expand to the SDeS rich side by 0.03.

In the micellar composition range ($X_2 = 0.78–1$), T_1 and T_2 values of protons of all the segments shorten as X_2 approaches 0.78. In the vesicle–micelle coexisting region, every T_1 continuously nears the vesicular one as the composition approaches 0.71. All T_1 values in the vesicle solution take almost the same value for all segmental protons regardless of the composition except at $X_2 = 0.70$.

T_1 of the sample at around $X_2 = 0.70$ is oddly longer than the other vesicular ones. This anomaly may be attributed to a bicontinuous (or sponge) phase. In the SDeS–DeTAB–H₂O system, transmission electron micrographs of the sample at $X_2 = 0.70$ and $m = 139$ mmol kg^{−1} show a spongelike structure as shown in Figure 9, although the sample had been initially assigned as in the vesicular phase because it is impossible to distinguish between vesicle and other bilayer-based structures by the surface tension measurement. Such a bicontinuous phase is believed to be found also in the D₂O system. The long T_1 values mean that surfactant molecules in the bicontinuous phase are less ordered than those in the vesicular phase. Similar behavior is observed in the T_1 and T_2 vs X_2 plots at $m = 152$ mmol kg^{−1}, though not shown here.

In Figure 10, panels a and b, T_1 and T_2 measured at 400 MHz for each segment are respectively plotted against X_2 at $m = 265$ mmol kg^{−1} with the broken lines to indicate the phase boundaries. T_1 and T_2 of all the protons in the micellar region

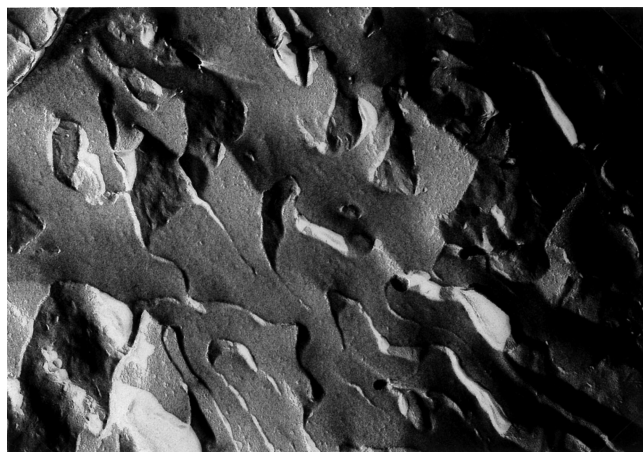


Figure 9. A FF-TEM image of a sponge structure formed in the SDeS-DeTAB-H₂O system at $X_2 = 0.70$ and $m = 139 \text{ mmol kg}^{-1}$. Scale bar = $0.5 \mu\text{m}$.

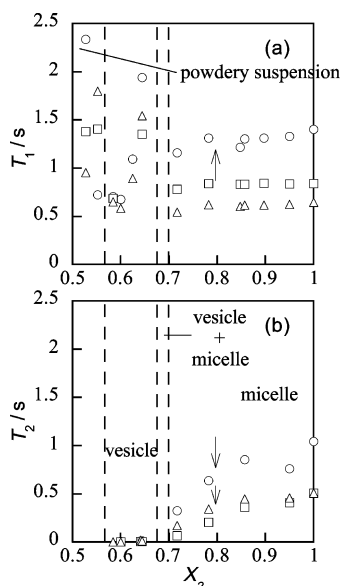


Figure 10. Relaxation times vs surfactant composition plots of the SDeS-DeTAB-D₂O system at $m = 265 \text{ mmol kg}^{-1}$ measured at 400 MHz: (a) spin-lattice relaxation time vs X_2 ; (b) spin-spin relaxation time vs X_2 ; (○) CH₃-; (□) -(CH₂)₇-; (Δ) -N(CH₃)₃; the dashed vertical lines indicate the phase boundaries; the plots bend slightly at the positions pointed out by the arrows.

shorten as X_2 approaches 0.5 similar to the case of $m = 100 \text{ mmol kg}^{-1}$. Furthermore, a slight bend is found at around $X_2 = 0.80$ on T_1 vs X_2 and T_2 vs X_2 curves. For this case of m , we also measured self-diffusion of the micelle. Dependence of the coefficient D on X_2 is shown in Figure 11. As for the self-diffusion of the micelle, D decreases with decreasing X_2 , showing a bend at around $X_2 = 0.80$, down to $6.24 \times 10^{-11} \text{ m}^2 \text{ s}^{-1}$ at $X_2 = 0.72$. Thus, at the same composition $X_2 \approx 0.80$, the decreasing rates with X_2 are enhanced for all cases of T_1 , T_2 , and D . As will be shown later in Figure 12d, the steep decreases in T_1 and T_2 at $X_2 < 0.8$ result from an increase in the slow correlation time τ_s ; namely, τ_s at $X_2 < 0.8$ is about twice as long as τ_s at $X_2 > 0.8$. In the micelle under consideration, all the anionic surfactant is considered to pair up with the cationic one. Since the number of DeS⁻-DeTA⁺ pairs increases with decreasing X_2 , it is considerably larger than that of unpaired DeTA⁺ in the range $X_2 = 0.7-0.8$. From the geometrical

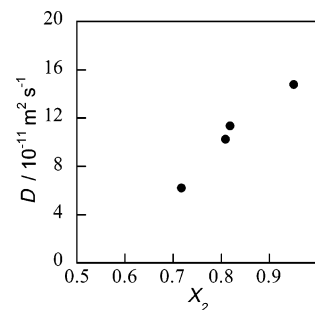


Figure 11. Self-diffusion coefficient vs surfactant composition at $m = 265 \text{ mmol kg}^{-1}$. A bend is seen around $X_2 = 0.8$, where sphere-rod transition of micelle occurs.

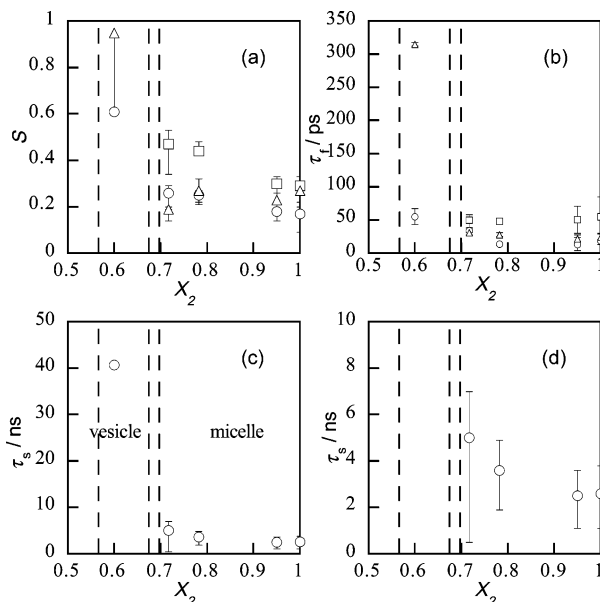


Figure 12. (a) Order parameter vs X_2 plots of the SDeS-DeTAB-D₂O system at $m = 265 \text{ mmol kg}^{-1}$; (b) fast correlation time vs X_2 ; (○) CH₃-; (□) -(CH₂)₇-; (Δ) -N(CH₃)₃; (c) slow correlation time vs X_2 ; (d) magnification of the micellar region of (c); the dashed vertical lines indicate the phase boundaries.

packing theory, therefore, it seems that the micelles in $X_2 = 0.7-0.8$ are of the rodlike shape rather than the spherical one. Namely, the paired molecules with a shape of a truncated cone mostly exist in the cylindrical part of the micelle and the excess DeTA⁺ ions form the end caps. Thus, it can be concluded that sphere-to-rod transition of the micelle takes place at around $X_2 = 0.8$. Both the increase in τ_s and the decrease in D in the range $X_2 = 0.7-0.8$ result from an increase in size of the micelle. If the effective radius R for the rodlike micelle is estimated from the experimental D by means of the Einstein-Stokes relation:

$$D = \frac{kT}{6\pi\eta R} \quad (9)$$

R is obtained to be 3.4 nm for $X_2 = 0.72$, while it is of the molecular length of the surfactants ($1.5-1.9 \text{ nm}$) for $X_2 = 0.8-1$.

As shown in Figure 10b, T_2 values of all the segments become extremely short suddenly with vesicle formation. Corresponding T_1 values become nearly constant irrespective of the composition or the segmental position except in $X_2 = 0.62-0.65$. The odd elongation of T_1 values in this composition range is probably due to the structural change of vesicle to a bicontinuous structure similar to the case of $m = 100 \text{ mmol kg}^{-1}$; $X_2 = 0.70$. These significant features of T_1 and T_2 bear much resemblance to the

dependence of T_1 and T_2 on the aggregation structure, vesicle or micelle, compared at the constant composition of $X_2 = 0.78$ shown in Figure 6.

Additionally, in the composition range $X_2 < 0.58$ T_1 values are scattered. This is most likely due to the flocculation of vesicle particles during the measurement. When a solution of $X_2 = 0.50$ – 0.58 is left to stand for ca. 10 min, it separates into a clear transparent solution at the bottom and a thicker suspension on top. In the present D_2O system, a powdery suspension of the same texture as that of the H_2O system is observed in the same region. The 1H NMR spectrum of the upper suspension is broader than that of a usual vesicle solution and T_1 could not be measured, whereas the spectrum and T_1 of the clear solution beneath are identical with those of a pure DeTAB monomer solution.

When T_1 of each segment in the vesicular region (except $X_2 = 0.62$ – 0.65) is compared with that in the micellar region, different trends between the segment in the hydrophilic headgroup and those in the hydrophobic tail are found. Namely, T_1 values of protons in the hydrophobic group are shorter in the vesicular region than in the micellar one, while T_1 values of protons in the hydrophilic headgroup are slightly longer in the former than in the latter. Such difference in the dependence of T_1 on X_2 between the hydrophilic and hydrophobic moieties is quantitatively explained based on the numerical values of τ_f , τ_s , and S .

S , τ_f , and τ_s are plotted against X_2 at $m = 265$ mmol kg^{-1} in panels a, b, and c of Figure 12, respectively. The broken lines show the phase boundaries and the parameters were estimated only in the micelle region and for the vesicle at $X_2 = 0.60$. T_1 and T_2 measurement on vesicle solutions at this total molality was successful only for the segments CH_3- and $-N(CH_3)_3$. Thus the order parameter and the correlation times were calculated only for these segments.

From Figure 12a, it is clear that all the segments become more ordered as X_2 approaches 0.5, and S drastically increases as micelles transform to vesicles. These large S values in the vesicle region also result from the considerably stronger constraint of the local and entire motions on the surfactant molecules as compared with that in micelle. With respect to the micellar region, S of $-(CH_2)_7-$ takes the largest values at all X_2 and shows the most prominent dependence on X_2 between the three segments. From this dependence of S on X_2 , we understand that molecules become well-ordered with increasing ratio of SDeS.

As exhibited in Figure 12b, τ_f scarcely changes with the surfactant composition in the micellar region, but τ_f of vesicle, especially for the proton of the hydrophilic group ($-N(CH_3)_3$), becomes much longer than the micellar ones. Hence, local motion of the surfactant in the vesicle is different from that in the micelle. From the results of S and τ_f , we understand that motion of the hydrophilic group of DeTAB is restricted due to pairing of DeS^- and $DeTA^+$ by the electrostatic interaction.

As one can see in Figure 12c, τ_s becomes long as X_2 approaches 0.5 from 1. All the anionic surfactant existing in the micelle is considered to pair up with the cationic one in the composition range $X_2 \geq 0.5$. Since the lateral diffusion of a DeS^- – $DeTA^+$ pair is slower than that of a single ionic surfactant in the micelle interior, the increased SDeS ratio makes the overall τ_s longer. Furthermore, the vesicle composition is at the most $X_2^V = 0.62$ whereas the micellar composition varies in the range $0.65 \leq X_2^M < X_2^2$. Therefore, there are many more DeS^- – $DeTA^+$ pairs in the vesicle. Consequently, the vesicular interior is considered to be much less fluid than the micellar

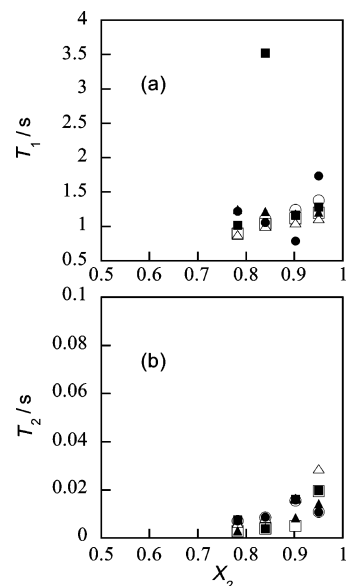


Figure 13. Relaxation times vs surfactant composition plots of the SDeS–DeTAB– D_2O system at $m = 30$ mmol kg^{-1} measured at 400 MHz: (a) spin–lattice relaxation time vs X_2 ; (b) spin–spin relaxation time vs X_2 ; (○) CH_3- ; (□) $-(CH_2)_7-$; (△) $-N(CH_3)_3$; open symbols represent experimental values and filled symbols represent recalculated values from S , τ_f , and τ_s .

one. In addition, the micellar region in Figure 12c is magnified in Figure 12d, and we see clearly that micellar τ_s depends on X_2 at constant m . τ_s of the spheroid micelle formed at $X_2 = 0.72$ is the largest, being twice as large as those of the spherical micelles.

T_1 values are predominantly determined by the local segmental motions because of the large values of τ_s in the present case; namely, one obtains $T_1^{-1} \approx 10A\tau_f(1 - S^2)$ from eq 6 for both micelles and vesicles. Therefore, T_1 becomes short with the increase in τ_f or the decrease in S . Both S and τ_f for the hydrophobic and hydrophilic groups in vesicle are larger than those in micelle owing to the increment of the DeS^- – $DeTA^+$ pairs and resultant strong electrostatic interaction between them. In the case of CH_3- , the effect of the enlarged S in the vesicle is surpassed by the increase in τ_f . Thus, T_1 in the vesicle becomes shorter ($T_1^{-1} \approx 3.6 \times 10^{-10} A s^{-1}$ with $\tau_s = 40$ ns, $\tau_f = 55$ ps, and $S = 0.6$) than in the micelle ($T_1^{-1} \approx 2.0 \times 10^{-10} A s^{-1}$ with $\tau_s = 5$ ns, $\tau_f = 20$ ps, and $S = 0.25$) because of the restriction of the local motion. On the other hand, S for $-N(CH_3)_3$ becomes nearly equal to 1.0 in the vesicle. This considerable increase in S cancels out the effect of the elongated τ_f . Therefore, because of the strong anchoring of the paired headgroup at the surface of the aggregate, T_1 in the vesicle becomes a little longer ($T_1^{-1} \approx 3.2 \times 10^{-10} A s^{-1}$ with $\tau_s = 40$ ns, $\tau_f = 310$ ps, and $S = 0.95$) than that in the micelle ($T_1^{-1} \approx 3.4 \times 10^{-10} A s^{-1}$ with $\tau_s = 5$ ns, $\tau_f = 35$ ps, and $S = 0.2$).

3.2.3. Effect of Composition Change on Dynamics of Vesicle. To examine how the dynamics of vesicle depends on X_2 , NMR relaxation measurement was carried out at $m = 30$ mmol kg^{-1} because at this total molality, vesicle is formed in a wide composition range. The results are shown in Figure 13a,b. The experimental T_1 and T_2 values shorten monotonically as X_2 approaches 0.5. Additionally, the relaxation times recalculated by eqs 6 and 7 from the order parameter and the correlation times well reproduce the experimental relaxation times. Therefore, the two-step model is applicable also to vesicles.

S , τ_f , and τ_s vs X_2 plots at $m = 30$ mmol kg^{-1} are illustrated in Figure 14, which are obtained from analyses of the relaxation

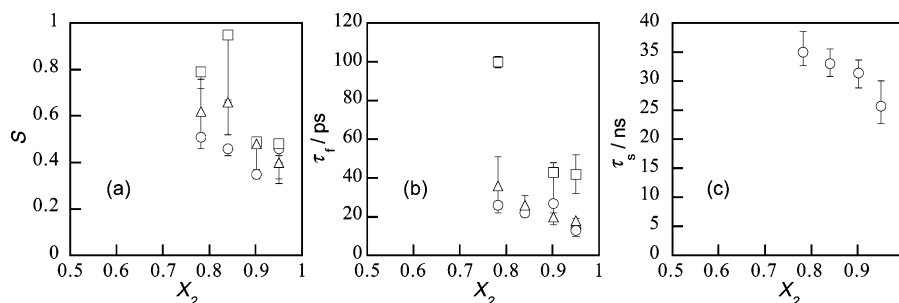


Figure 14. (a) Order parameter vs X_2 plots of the SDeS–DeTAB–D₂O system at $m = 30 \text{ mmol kg}^{-1}$; (b) fast correlation time vs X_2 ; (○) CH₃–; (□) –(CH₂)₇–; (Δ) –N(CH₃)₃; (c) slow correlation time vs X_2 .

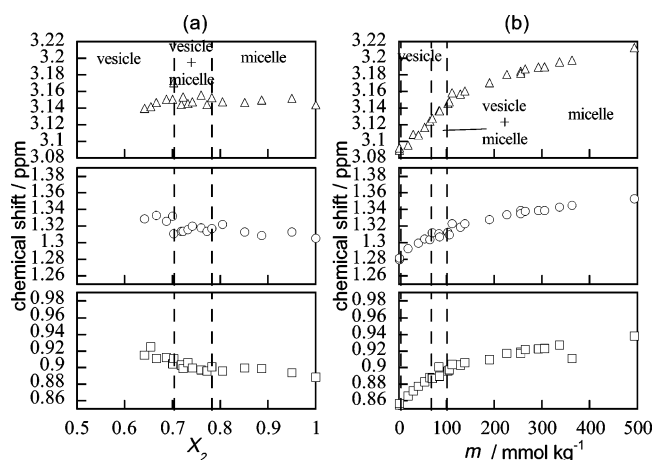


Figure 15. (a) Chemical shifts vs X_2 plots of the SDeS–DeTAB–D₂O system at $m = 100 \text{ mmol kg}^{-1}$; (b) chemical shifts vs m plots at $X_2 = 0.78$; (○) CH₃–; (□) –(CH₂)₇–; (Δ) –N(CH₃)₃; the dashed vertical lines indicate the phase boundaries.

data shown in Figure 13. At all the compositions, τ_f increases in the order $-\text{N}(\text{CH}_3)_3 \sim \text{CH}_3- < -(\text{CH}_2)_7-$ and S , $\text{CH}_3- < -\text{N}(\text{CH}_3)_3 \sim -(\text{CH}_2)_7-$. The dependence of τ_f on the segment position and on X_2 for these vesicles is similar to those for the micelles examined at higher total molalities as seen in Figure 12. Moreover, τ_f elongates as X_2 decreases.

S and τ_s also increase as X_2 approaches 0.5 from 1. This behavior is explained as follows. At higher X_2 , the vesicle composition X_2^V is slightly larger than 0.5, whereas $X_2^V \sim 0.5$ near $X_2 = 0.5$. Hence there are more DeTA⁺ ions than DeS[–] in the vesicle of $X_2 = 0.95$ and the vesicle particle is slightly charged cationically and its curvature becomes larger than the vesicle of $X_2^V = 0.5$. Therefore, the number density of surfactant molecules per vesicle particle is lower and the number of DeS[–]–DeTA⁺ pairs is fewer for the former than the latter. As also shown by Figure 3, vesicular size and the number of SDeS[–]–DeTA⁺ pairs increase as X_2 decreases. The tumbling of vesicle particles becomes slower due to growth of vesicular size and diffusion of surfactant molecules in the vesicle becomes slower by pairing of DeS[–] and DeTA⁺ ions and consequently the fraction of contribution of the slow motion becomes larger as X_2 approaches 0.5.

3.3. Chemical Shifts. Finally, let us briefly mention dependence of the chemical shifts on X_2 at constant m and that on m at constant X_2 . The origin of the variation in the chemical shift is a change in the shielding by electron clouds about each nucleus. Strong shielding by the change of the molecular environment can shift the resonant frequency to a lower magnetic field. Chemical shifts of the protons are plotted against X_2 at $m = 100 \text{ mmol kg}^{-1}$ in Figure 15a and are plotted against m at $X_2 = 0.78$ in Figure 15b together with the broken lines to

indicate the phase boundaries. Surfactants exist as monomers only in the very low concentration range between the vertical axis and the broken line drawn next to it in Figure 15b. There, it is clearly seen that the protons in monomer surfactant resonate in the highest magnetic field. Moreover, as one can see in Figure 15a, chemical shifts of –(CH₂)₇– and CH₃– segments in the vesicle are observed in the lower magnetic field than those in the micelle, while the chemical shift of the –N(CH₃)₃ segment is almost constant. Therefore, it is considered that the hydrophobic tails of the surfactants are aligned more closely to each other in the vesicle particle than in the micelle particle.

On the other hand, as shown in Figure 15b, chemical shift values increase with m . Since the monomer contribution to the chemical shifts is negligible in this case, the increment of the chemical shifts is attributable to deformation of the cloud of electrons around the protons. Because the surfactants are ionic, the Debye length is reduced at high total concentration thereby allowing closer molecular packings of the surfactants in the vesicle or micelle particles.

4. Conclusion

This study shows that the combination of thermodynamic information (phase diagram of aggregate formation) and relaxation experiments gives correct interpretation on the molecular motion in the aggregates, and one can compare the molecular motion of surfactants in micelles and vesicles at various compositions or total molalities. The following are found on the SDeS–DeTAB–D₂O system. With micelle or vesicle formation, the molecular motion becomes slower than the monomer one. Especially, the vesicle is large in size and consists of many DeS[–]–DeTA⁺ pairs; consequently, mobilities of the vesicle particle and molecules inside it are considerably low.

The shift of the resonant frequency to the lower magnetic field observed for the micellar and vesicular solutions reflects the fact that surfactant molecules are constrained near each other in the micelle and vesicle particles. It is also shown that in the high concentration range, surfactant molecules are more tightly arrayed.

Acknowledgment. M.V. thanks Prof. Dr. Heiz Hoffmann of Bayreuth University for the opportunity to do TEM experiments and Dr. Youhei Kawabata and Prof. Tadashi Kato of Tokyo Metropolitan University for their great help in the light scattering measurement. This study was supported by Grant-in-Aid for Young Researchers (B), No. 15750002, from the Ministry of Education, Science, Culture and Sports of Japan.

References and Notes

- (1) Kaler, E. W.; Murthy, A. K.; Rodriguez, B.; Zasadzinski, J. A. N. *Science* **1989**, *245*, 1371.
- (2) Villeneuve, M.; Kaneshina, S.; Imae, T.; Aratono, M. *Langmuir* **1999**, *15*, 2029.

- (3) Söderman, O.; Herrington, K. L.; Kaler, E. W.; Miller, D. D. *Langmuir* **1997**, *13*, 5531.
- (4) Wennerström, H.; Lindman, B.; Söderman, O.; Drakenberg, T.; Rosenholm, J. B. *J. Am. Chem. Soc.* **1979**, *101*, 6860.
- (5) Halle, B.; Wennerström, H. *J. Chem. Phys.* **1981**, *75*, 1928.
- (6) Eriksson, P.-O.; Khan, A.; Lindblom, G. *J. Phys. Chem.* **1982**, *86*, 387.
- (7) Söderman, O.; Walderhaug, H.; Henriksson, U.; Stilbs, P. *J. Phys. Chem.* **1985**, *89*, 3693.
- (8) Ellena, J. F.; Dominey, N.; Cafiso, D. S. *J. Phys. Chem.* **1987**, *91*, 131.
- (9) Canet, D.; Turki, T.; Belmajdoub, A.; Diter, B. *J. Phys. Chem.* **1988**, *92*, 1219.
- (10) Nusselder, J.-J. H.; Engberts, J. B. F. N. *J. Phys. Chem.* **1989**, *93*, 6142.
- (11) Regev, O.; Kang, C.; Khan, A. *J. Phys. Chem.* **1994**, *98*, 6619.
- (12) Shikata, T.; Morishima, Y. *Langmuir* **1997**, *13*, 1931.
- (13) Lipari, G.; Szabo, A. *J. Am. Chem. Soc.* **1982**, *104*, 4546.
- (14) Dreger, E. E.; Keim, G. I.; Miles, G. D.; Shedlonsky, L.; Ross, J. *Ind. Eng. Chem.* **1944**, *36*, 610.
- (15) Abragam, A. *The Principles of Nuclear Magnetism*; Clarendon: Oxford, UK, 1961.
- (16) Villeneuve, M.; Kaneshina, S.; Aratono, M. *J. Colloid Interface Sci.* **2003**, *262*, 227.
- (17) Kaler, E. W.; Herrington, K. L.; Murthy, A. K.; Zasadzinski, J. A. N. *J. Phys. Chem.* **1992**, *96*, 6698.
- (18) Néry, H.; Söderman, O.; Canet, D.; Walderhaug, H.; Lindman, B. *J. Phys. Chem.* **1986**, *90*, 5802.
- (19) Walderhaug, H.; Söderman, O.; Stilbs, P. *J. Phys. Chem.* **1984**, *88*, 1655.